J|A|C|S
ARTICLES
Published on Web 03/31/2007

Hybrid Gadolinium Oxide Nanoparticles: Multimodal Contrast Agents for in Vivo Imaging

Jean-Luc Bridot,[†] Anne-Charlotte Faure,[†] Sophie Laurent,[‡] Charlotte Rivière,*[,§] Claire Billotey,[||] Bassem Hiba,[||] Marc Janier,[||] Véronique Josserand,[⊥] Jean-Luc Coll,[⊥] Luce Vander Elst,[‡] Robert Muller,[‡] Stéphane Roux,*[,†] Pascal Perriat,[#] and Olivier Tillement[†]

Contribution from the Laboratoire de Physico-Chimie des Matériaux Luminescents, UMR 5620 CNRS—Université Claude Bernard Lyon 1, 69622 Villeurbanne Cedex, France, Department of General, Organic and Biomedical Chemistry, NMR and Molecular Imaging Laboratory, University of Mons-Hainaut, 7000 Mons, Belgium, Nano-H SAS, 23 rue Royale, 69001 Lyon, France, Laboratoire CREATIS—Animage, UMR 5515 CNRS-U630 INSERM-INSA de Lyon—Université Claude Bernard Lyon 1, 69622 Villeurbanne Cedex, France, Groupe de Recherche sur le Cancer du Poumon, INSERM U578, Institut Albert Bonniot, 38706 La Tronche Cedex, France, and Groupe d'Etudes de Métallurgie Physique et de Physique des Matériaux, UMR 5510 CNRS—INSA de Lyon, 69621 Villeurbanne Cedex, France

Received November 21, 2006; E-mail: roux@pcml.univ-lyon1.fr; charlotte.riviere@lpmcn.univ-lyon1.fr

Abstract: Luminescent hybrid nanoparticles with a paramagnetic Gd_2O_3 core were applied as contrast agents for both in vivo fluorescence and magnetic resonance imaging. These hybrid particles were obtained by encapsulating Gd_2O_3 cores within a polysiloxane shell which carries organic fluorophores and carboxylated PEG covalently tethered to the inorganic network. Longitudinal proton relaxivities of these particles are higher than the positive contrast agents like Gd−DOTA which are commonly used for clinical magnetic resonance imaging. Moreover these particles can be followed up by fluorescence imaging. This study revealed that these particles suited for dual modality imaging freely circulate in the blood vessels without undesirable accumulation in lungs and liver.

Introduction

The intense research activities devoted to the nanoparticles during the past decade have opened the door to promising biological and medical applications.[1] Besides their reduced size which makes them suitable for labeling biomolecules or for exploring the living machinery at the subcellular scale without functional alteration,[2] the great potential of the nanoparticles rests on the ability to gather in a same object several complementary properties. This was illustrated by the pioneering works of Weissleder's group that led to the development of triple label nanoparticles suited for the in vivo tracking of labeled cells.[3] They are composed of a superparamagnetic iron oxide core (5 nm) encapsulated in a dextran shell (thickness: 20 nm) which allows the derivatization of the particles both by fluorescent TAT peptides and by radioisotope ^{111}In chelates. The functionalization of these particles by TAT peptide facilitates their internalization in cells that is successfully followed up by fluorescence imaging (FI), magnetic resonance imaging (MRI), and by nuclear imaging. Such a combination of several detection techniques, that the use of multimodal particulate agents made possible, ensures a better reliability of the collected data. As a result, benefits can be expected for in vivo small-animal imaging which is a prerequisite step before clinical application but also a very useful tool for biomedical investigation. Because of the great repercussions on the clinical diagnosis and on surgical protocol, the development of multimodal contrast agents for in vivo imaging is a rapidly growing field.[4] Particularly, nanoparticles combining fluorescence and magnetic resonance imaging received much attention because they ally the high sensitivity of the fluorescence phenomenon to the high spatial resolution of MRI. Contrary to the fluorescence imaging whose in vivo application is seriously limited because of the weak penetration depth of light, MRI has become a prominent technique in diagnostic clinical medicine owing to the possibility of getting highly resolved three-dimensional images of living bodies.[5] Moreover this technique contributes to improving the comfort

[†] Laboratoire de Physico-Chimie des Matériaux Luminescents, Université Claude Bernard Lyon 1.
[‡] University of Mons-Hainaut.
[§] Nano-H SAS.
[||] Laboratoire CREATIS, Université Claude Bernard Lyon 1
[⊥] Institut Albert Bonniot.
[#] Groupe d'Etudes de Métallurgie Physique et de Physique des Matériaux, INSA de Lyon.

(1) (a) Brigger, I.; Dubernet, C.; Couvreur, P. *Adv. Drug Delivery Rev.* **2002**, *54*, 631−651. (b) Sunderland, C. J.; Steiert, M.; Talmadge, E. J.; Derfus, M. A.; Barry, S. E. *Drug Dev. Res.* **2006**, *67*, 70−93. (c) Whitesides, G. M. *Nat. Biotechnol*. **2003**, *21*, 1161−1165. (d) Ferrari, M. *Nat. Rev.* **2005**, *5*, 161−171.
(2) Medintz, I. L.; Uyeda, H. T.; Goldman, E. R.; Mattoussi, H. *Nat. Mater.* **2005**, *4*, 435−446.
(3) Lewin, M.; Carlesso, N.; Tung, C. H.; Tang, X. W.; Cory, D.; Scadden, D. T.; Weissleder, R. *Nat. Biotechnol.* **2000**, *18*, 410−414.
(4) Kircher, M. F.; Mahmood, U.; King, R. S.; Weissleder, R.; Josephson, L. *Cancer Res.* **2003**, *63*, 8122−8125.
(5) Caravan, P. *Chem. Soc. Rev.* **2006**, *35*, 512−523.

10.1021/ja068356j CCC: $37.00

of the patient because it is noninvasive, rapid, and avoids the use of radiochemicals.[6] The MRI technique relies upon the relaxation of water protons which depends on the magnetic fields (the strong static magnetic field $\mathbf{B}_0$ and the radiofrequency-field), on the pulse sequence, and on the heterogeneous distribution and environment of water in organism. The interpretation of the resulting images leads therefore to the delineation and the identification of most tissues. The contrast can be enhanced by the use of contrast agents that can be divided into two groups, the negative and the positive contrast agents.[7] Negative contrast agents, which are essentially formed of superparamagnetic iron oxide nanoparticles, induce a large shortening of the transverse relaxation time T_2 leading to a darkening of the MR images, whereas the close contact of water molecules with positive contrast agents is revealed by a brightness which reflects the shortening of the longitudinal relaxation time T_1.[7] Because of the particulate structure of most negative contrast agents, supplementary features (luminescence, targeting) can easily be added either by embedding them in a functionalized organic (dextran, amphiphilic shell) or inorganic (polysiloxane) polymer or by using dimercaptosuccinic acid or cathechol derivatives as surface passivating agents and grafting sites for fluorescent molecules and biotargeting groups.[3,8] The literature is therefore overflowing with multimodal superparamagnetic iron oxide nanoparticles which at least combine fluorescence imaging and MRI. The development of multimodal positive contrast agents was impeded because they were mainly based on the chelates of metal ions with a large number of unpaired electrons such as Gd^{3+} (seven unpaired electrons). Indeed their molecular structure makes their functionalization by fluorophores more difficult. Moreover their low molecular weight impedes their accumulation in an organism for a sufficiently long time: they are quickly removed by renal excretion.[9] In addition, the nonspecificity of gadolinium complexes[10] and their short rotational correlation time[11] which limits the proton relaxivity led to the development of more efficient contrast agents. Several attractive strategies were explored aiming the synthesis of Gd(III) based agents with a higher molecular weight. To achieve this goal, Gd−DTPA or -DOTA functionalized polymer,[12] self-assembled peptide amphiphiles[13] or viral capsid,[14] Gd−DTPA terminated dendrimer,[15] gadolinium complexes loaded liposomes,[16] high-density lipoprotein nanoparticles,[17] micelles,[18] or polymeric nanoparticles,[19] gadolinium ions entrapped in zeolites,[20] fullerenes,[21] carbon nanotubes,[22] clays[23] or mesoporous silica nanoparticles,[24] and gadolinium chelates immobilized on quantum dots,[25] on lipid particles,[26] and on gold nanoparticles[27] were synthesized and studied. They are all characterized by an increase of the molecular weight and of the amount of Gd(III) ions per contrast agent. As a consequence of their structure, some of them were easily functionalized by biotargeting groups and/or fluorescent molecules conferring them additional attractive features.[12a,14−17,25,26] Although the number of gadolinium atoms is very high even for smaller size, the potential of crystalline nanoparticles based on inorganic or organometallic compounds of gadolinium such as gadolinium oxide,[28] gadolinium fluoride nanoparticles,[29] and nanorods composed of a metal−organic frameworks built from gadolinium ions and organic bridging ligands (1,4-benzenedicarboxylate)[30] has been only recently evaluated. These nanometric objects exhibit relaxivities r_1, which refers to the amount in $1/T_1$ per millimole of agent, higher than the gadolinium chelates do. However their size is relatively high, they were not functionalized for biological

(6) Bottrill, M.; Kwok, L.; Long, N. J. *Chem. Soc. Rev.* **2006**, *35*, 557−571.
(7) (a) Aimé, S.; Botta, M.; Terreno, E. *Adv. Inorg. Chem.* **2005**, *57*, 173−237. (b) Caravan, P.; Ellison, J. J.; McMurry, T. J.; Lauffer, R. B. *Chem. Rev.* **1999**, *99*, 2293−2352. (c) Merbach, A.; Tóth, E. *The Chemistry of Contrast Agents in Magnetic Resonance Imaging*; John Wiley and Sons: Chichester, U.K., 2001.
(8) (a) Nasongkla, N.; Bey, E.; Ren, J.; Ai, H.; Khemtong, C.; Guthi, J. S.; Chin, S. F.; Sherry, A. D.; Boothman, D. A.; Gao, J. *Nano Lett.* **2006**, *6*, 2427−2430. (b) Bertorelle, F.; Wilhelm, C.; Roger, J.; Gazeau, F.; Ménager, C.; Cabuil, V. *Langmuir* **2006**, *22*, 5385−5391. (c) Veiseh, O.; Sun, C.; Gunn, J.; Kohler, N.; Gabikian, P.; Lee, D.; Bhattarai, N.; Ellenbogen, R.; Sze, R.; Hallahan, A.; Olson, J.; Zhang, M. *Nano Lett*. **2005**, *5*, 1003−1008. (d) Jun, Y. W.; Huh, Y. M.; Choi, J. S.; Lee, J. H.; Song, H. T.; Kim, S.; Yoon, S.; Kim, K. S.; Shin, J. S.; Suh, J. S.; Cheon, J. *J. Am. Chem. Soc.* **2005**, *127*, 5732−5733. (e) Wang, L.; Yang, Z.; Gao, J.; Xu, K.; Gu, H.; Zhang, B.; Zhang, X.; Xu, B. *J. Am. Chem. Soc.* **2006**, *128*, 13358−13359. (f) Xu, C.; Xu, K.; Gu, H.; Zheng, R.; Liu, H.; Zhang, X.; Guo, Z.; Xu, B. *J. Am. Chem. Soc.* **2004**, *126*, 9938−9939.
(9) Schmiedl, U.; Moseley, M. E.; Ogan, M. D.; Chew, W. D.; Brasch, R. C. *J. Comput. Assist. Tomogr.* **1987**, *11*, 306−313.
(10) Morawski, A. M.; Lanza, G. A.; Wickline, S. A. *Curr. Opin. Biotechnol.* **2005**, *16*, 89−92.
(11) Fatin-Rouge, N.; Tóth, E.; Meuli, R.; Bünzli, J.-C. G. *J. Alloys Compd.* **2004**, *374*, 298−302.
(12) (a) Hüber, M. M.; Staubli, A. B.; Kustedjo, K.; Gray, M. H. B.; Shih, J.; Fraser, S. E.; Jacobs, R. E.; Meade, T. J. *Bioconjugate Chem.* **1998**, *9*, 242−249. (b) Yan, G. P.; Liu, M. L.; Li, L. Y. *Bioconjugate Chem.* **2005**, *16*, 967−971.
(13) (a) Bull, S. R.; Guler, M. O.; Bras, R. E.; Meade, T. J.; Stupp, S. I. *Nano Lett.* **2005**, *5*, 1−4. (b) Bull, S. R.; Guler, M. O.; Bras, R. E.; Venkatasubramanian, P. N.; Stupp, S. I.; Meade, T. J. *Bioconjugate Chem.* **2005**, *16*, 1343−1348.
(14) Anderson, E. A.; Isaacman, S.; Peabody, D. S.; Wang, E. Y.; Canary, J. W.; Kirshenbaum, K. *Nano Lett.* **2006**, *6*, 1160−1164.
(15) (a) Langereis, S.; de Lussanet, Q. G.; van Genderen, M. H. P.; Backes, W. H.; Meijer, E. W. *Macromolecules* **2004**, *37*, 3084−3091. (b) Talanov, V. S.; Regino, C. A. S.; Kobayashi, H.; Bernardo, M.; Choyke, P. L.; Brechbiel, M. W. *Nano Lett.* **2006**, *6*, 1459−1463.
(16) Mulder, W. J. M.; Strijkers, G. J.; Griffioen, A. W.; van Bloois, L.; Molema, G.; Storm, G.; Koning, G. A.; Nicolay, K. *Bioconjugate Chem.* **2004**, *15*, 799−806.
(17) (a) Frias, J. C.; Williams, K. J.; Fisher, E. A.; Fayad, Z. A. *J. Am. Chem. Soc.* **2004**, *126*, 16316−16317. (b) Frias, J. C.; Ma, Y.; Williams, K. J.; Fayad, Z. A.; Fisher, E. A. *Nano Lett.* **2006**, *6*, 2220−2224.
(18) (a) Accordo, A.; Tesauro, D.; Roscigno, P.; Gianolio, E.; Paduano, L.; D'Errico, G.; Pedone, C.; Morelli, G. *J. Am. Chem. Soc.* **2004**, *126*, 3097−3107. (b) Parac-Vogt, T. N.; Kimpe, K.; Laurent, S.; Piérart, C.; Vander Elst, L.; Muller, R. N.; Binnemans, K. *Eur. J. Inorg. Chem.* **2004**, *17*, 3538−3543.
(19) (a) Reynolds, C. H.; Annan, N.; Beshah, K.; Huber, J. H.; Shaber, S. H.; Lenkinski, R. E.; Wortman, J. A. *J. Am. Chem. Soc.* **2000**, *122*, 8940−8945. (b) Turner, J. L.; Pan, D.; Plummer, R.; Chen, Z.; Wittaker, A. K.; Wooley, K. L. *Adv. Funct. Mater.* **2005**, *15*, 1248−1254.
(20) Platas-Iglesias, C.; Vander Elst, L.; Zhou, W.; Muller, R. N.; Geraldes, C. F. G. C.; Maschmeyer, T.; Peters, J. A. *Chem.—Eur. J.* **2002**, *8*, 5121−5131.
(21) Tóth, E.; Bolskar, R. D.; Borel, A.; Gonzalez, G.; Helm, L.; Merbach, A. E.; Sitharaman, B.; Wilson, L. J. *J. Am. Chem. Soc.* **2005**, *127*, 799−805.
(22) Sitharaman, B.; Kissell, K. R.; Hartman, K. B.; Tran, L. A.; Baikalov, A.; Rusakova, I.; Sun, Y.; Khant, H. A.; Ludtke, S. J.; Chiu, W.; Laus, W.; Tóth, E.; Helm, L.; Merbach, A. E.; Wilson, L. J. *Chem. Commun.* **2005**, 3915−3917.
(23) Balkus, K. J., Jr.; Shi, J. *Langmuir* **1996**, *12*, 6277−6281.
(24) Lin, Y. S.; Hung, Y.; Su, J. K.; Lee, R.; Chang, C.; Lin, M. L.; Mou, C. Y. *J. Phys. Chem. B* **2004**, *108*, 15608−15611.
(25) (a) Mulder, W. J. M.; Koole, R.; Brandwijk, R. J.; Storm, G.; Chin, P. T. K.; Strijkers, G. J.; de Mello Donega, C.; Nicolay, K.; Griffioen, A. W. *Nano Lett.* **2006**, *6*, 1−6. (b) van Tilborg, G. A. F.; Mulder, W. J. M.; Chin, P. T. K.; Storm, G.; Reutelingsperger, C. P.; Nicolay, K.; Strijkers, G. J. *Bioconjugate Chem.* **2006**, *17*, 865−868.
(26) Vuu, K.; Xie, J.; McDonald, M. A.; Bernardo, M.; Hunter, F.; Zhang, Y.; Li, K.; Bednarski, M.; Guccione, S. *Bioconjugate Chem.* **2005**, *16*, 995−999.
(27) Debouttière, P.-J.; Roux, S.; Vocanson, F.; Billotey, C.; Beuf, O.; Favre-Réguillon, A.; Lin, Y.; Pellet-Rostaing, S.; Lamartine, R.; Perriat, P.; Tillement, O. *Adv. Funct. Mater.* **2006**, *16*, 2330−2339.
(28) (a) MacDonald, M. A.; Watkin, K. L. *Invest. Radiol.* **2003**, *38*, 305−310. (b) Engström, M.; Klasson, A.; Pedersen, H.; Vahlberg, C.; Käll, P. O.; Uvdal, K. *Magn. Reson. Mater. Phys.* **2006**, *19*, 180−186. (c) Roberts, D.; Zhu, W. L.; Frommen, C. M.; Rosenzweig, Z. *J. Appl. Phys.* **2000**, *87*, 6208. (d) Perriat, P.; Louis, C.; Marquette, C. A.; Bazzi, R.; Roux, S.; Tillement, O.; Ledoux, G. Hybrid Nanoparticles Comprising a Core of Rare Earth Sesquioxide Carrying Biological Ligands. PCT/Fr2005/000491.
(29) Evanics, F.; Diamente, P. R.; van Veggel, F. C. J. M.; Stanisz, G. J.; Prosser, R. S. *Chem. Mater.* **2006**, *18*, 2499−2505.
(30) Rieter, W. J.; Taylor, K. M. L.; An, H.; Lin, W.; Lin, W. *J. Am. Chem. Soc.* **2006**, *128*, 9024−9025.

applications or for a multimodal detection, and no in vivo studies were undertaken. In a previous paper, we described the synthesis of doubly luminescent hybrid nanoparticles with a diameter in the 10−20 nm range for the biological labeling.[31] They were obtained by embedding the crystalline gadolinium oxide core (doped by the highly photostable luminescent Tb^{3+} ions) by a polysiloxane shell whose inner part is functionalized by organic fluorophores characterized by a transient but intense luminescence and the outer part is derivatized by biotargeting groups such as streptavidine or nucleic acids. The capability of these hybrid particles to be used as positive contrast agents for MRI which was suggested in the previous paper has been investigated. The present study focused on the influence of the purification steps and of the gadolinium oxide core size on the shortening of T_1 relaxation time (in other words, on the MR images contrast) and on their follow-up after intravenous injection in living organisms (mice and rats) monitored by fluorescence and MR imaging.

Experimental Section

Chemicals. Gadolinium chloride hexahydrate (99.99%), sodium hydroxide (99.99%), tetraethyl orthosilicate ($Si(OC_2H_5)_4$, TEOS, 98%), (3-aminopropyl)triethoxysilane ($H_2N(CH_2)_3$-$Si(OC_2H_5)_3$, APTES, 99%), fluorescein isothiocyanate (FITC, 90%), rhodamine B isothiocyanate (RBITC), 1-(3-dimethylaminopropyl)-3-ethylcarbodiimide hydrochloride (EDC, 98+%), pentafluorophenol (PFP, 99%), poly(ethylene glycol)bis(carboxymethyl)ether 250 $g \cdot mol^{-1}$ ($PEG(COOH)_2$, 99%), hepes solution (solution in water, pH 7.0−7.6), sodium chloride, triethylamine (TEA, 99.5%), and hydrochloric acid (HCl, 37%) were purchased from Aldrich Chemical (France). Cy5 mono-NHS-ester (89.1%) was purchased from Amersham Bioscience. Ethanol, diethylene glycol (DEG, 99%), and other organic solvents (reagent grade) were purchased from SDS (France) and used as received. For the preparation of an aqueous solution of nanoparticles, only milli-Q water ($\rho > 18$ MΩ) was used. The dialysis of colloidal solutions was performed with tubular membrane of cellulose (MWCO = 4−6 kDa) purchased from Roth (France).

Synthesis of Gadolinium Oxide Nanoparticles Embedded in a Polysiloxane Shell. These particles were obtained by a two-step route. Gadolinium oxide nanoparticles were first synthesized by applying a modified "polyol" protocol.[32] Afterward a polysiloxane shell growth was induced by hydrolysis−condensation of convenient siloxane precursors in presence of the nanoparticles.[31]

Preparation of Gadolinium Oxide Core. Gadolinium chloride salt (11.53 g) was placed in 200 mL of DEG at 60 °C under vigorous stirring overnight. Sodium hydroxide solution (7.5 mL, 3 M) was added and the solution was heated at 140 °C for 1 h and at 180 °C for 4 h. A transparent colloid of gadolinium oxide nanoparticles was obtained and can be stored at room temperature for weeks without alteration.

Preparation of Larger Gd_2O_3 Nanoparticles. Gadolinium chloride salt (9.80 g) was placed in 150 mL of DEG at 60 °C under vigorous stirring overnight. A solution (50 mL) containing nanoparticles of 2.2 or 3.8 nm was added. Sodium hydroxide solution (7.5 mL, 3 M) was added and the solution was heated at 140 °C for 1 h and at 180 °C for 4 h. A transparent colloid of gadolinium oxide nanoparticles was obtained and can be stored at room temperature for weeks without alteration.

Encapsulation of Gd_2O_3 Cores by Polysiloxane Shell. A solution containing organic dyes (FITC (1.2 mg), RBITC (1.6 mg), or Cy5 NHS ester (5 mg)) and 1.4 μL of APTES dissolved in 291 μL of DMSO was prepared as a precursor and stirred overnight. The coupling reaction between the organic fluorophores and APTES was certified by mass spectrometry with complete disappearance of the molecular peak of the fluorophore (m/z = 390.2, 500.3, 792.0 for FITC, RBITC, and Cy5, respectively) and the appearance of the molecular peak of the fluorophore conjugated APTES (m/z = 611.1, 721.2, 858.3 for FITC-, RBITC-, and Cy5-APTES, respectively). Organic dyes conjugated APTES solution and a portion of 327 μL of APTES and of 209 μL of TEOS were added to 1.5 mL of solution containing Gd_2O_3 nanoparticles diluted in 13.5 mL of DEG under stirring at 40 °C. After 1 h, a portion of 792 μL of a DEG solution (0.1 M of TEA, 10 M of water) was added. The other portions of polysiloxane precursors and of hydrolysis solution were sequentially and alternatively added. The final mixture was stirred for 48 h at 40 °C.

Purification. Purification of naked and polysiloxane-coated nanoparticles was performed by dialysis against ethanol. The colloidal solution (20 mL) was introduced in a tubular membrane of cellulose (MWCO = 4−6 kDa) and immersed in 250 mL of ethanol which was replaced every 24 h for 3 days. A fourth stage of dialysis can eventually be carried out for 4 days. For the preparation of a stem solution which is stable for weeks, 3 mL of DEG were added to the purified solution, and ethanol was eliminated under reduced pressure. For the transfer of the polysiloxane-coated nanoparticles in water, the colloid in ethanol was dialyzed against water.

Covalent Grafting of Poly(ethylene glycol)bis(carboxymethyl)-ether on Hybrid Nanoparticles. x moles of 0.091 M poly(ethylene glycol)bis(carboxymethyl)ether (250 $g \cdot mol^{-1}$, $PEG(COOH)_2$) in DEG were added to isopropanol solution containing $2x$ moles of EDC and $2x$ moles of PFP (0.367 M). The mixture was stirred for 1.5 h at room temperature. The reaction between COOH groups of the polymer and PFP, assisted by EDC, is expected to yield pentafluorophenyl esters.[33] The covalent grafting of PEG onto the hybrid nanoparticles was performed by the addition of pentafluorophenyl ester modified PEG in DEG solution containing hybrid nanoparticles (x/12000 mol, 7.5 μM). This solution was stirred for 12 h at room temperature. Afterward the colloid was dialyzed for 48 h against water (1:20, v/v) which was renewed three times.

High-Resolution Transmission Electron Microscopy. HRTEM was used to obtain detailed structural and morphological information about the samples and was carried out using a JEOL 2010 microscope operating at 200 kV. The samples for HRTEM were prepared by depositing a drop of a diluted colloidal solution on a carbon grid and allowing the liquid to dry in air at room temperature.

Size Measurement. Direct measurement of the size distribution of the nanoparticles suspended in the polyol medium was performed via Zetasizer 3000 HSa and Zetasizer NanoS PCS (photon correlation spectroscopy) from Malvern Instrument. Measurements were directly taken on the colloid after synthesis or surface modification in DEG.

ζ-Potential Measurements. Direct determination of the ζ-potential of the hybrid nanoparticles were performed via a Zetasizer 3000 HSa (laser He-Ne (633 nm)) from Malvern Instrument. Prior to the experiment, the sol was diluted in an aqueous solution containing 0.01 M NaCl and adjusted to the desired pH.

Inductively Coupled Plasma−Mass Spectrometry (ICP−MS) Analysis. Determination of the gadolinium content in a sample was performed by ICP−MS analysis (with a Thermo Elemental serie X7 VG X7 CCT). Before measuring Gd concentration, samples of colloidal solution were diluted in 0.5 M HNO_3 (1:2500, v/v) and in HNO_3 (2%, 2ppb In; 1:50, v/v).

(31) Louis, C.; Bazzi, R.; Marquette, C. A.; Bridot, J.-L.; Roux, S.; Ledoux, G.; Mercier, B.; Blum, L.; Perriat, P.; Tillement, O. *Chem. Mater.* **2005**, *17*, 1673−1682.

(32) (a) Bazzi, R.; Flores-Gonzalez, M.; Louis, C.; Lebbou, K.; Dujardin, C.; Brenier, A.; Zhang, W.; Tillement, O.; Bernstein, E.; Perriat, P. *J. Lumin.* **2003**, *102*−*103*, 445−450. (b) Bazzi, R.; Flores, M. A.; Louis, C.; Lebbou, K.; Zhang, W.; Dujardin, C.; Roux, S.; Mercier, B.; Ledoux, G.; Bernstein, E.; Perriat, P.; Tillement, O. *J. Colloid Interface Sci.* **2004**, *273*, 191−197.

(33) (a) Adamczyk, M.; Fishpaugh, J. R.; Mattingly, P. G. *Tetrahedron Lett.* **1995**, *36*, 8345−8346. (b) Kovacs, J.; Mayers, G. L.; Johnson, R. H.; Cover, R. E.; Ghatak, U. R. *J. Org. Chem.* **1970**, *35*, 1810−1815.

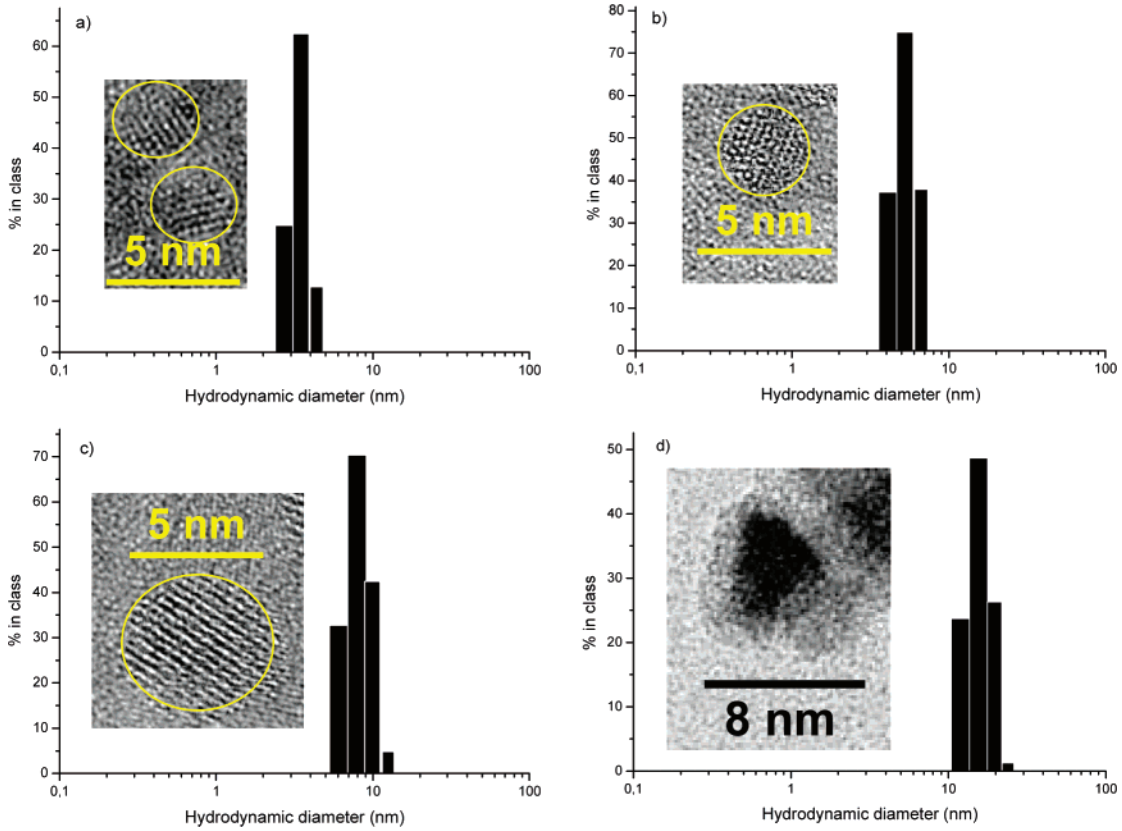

Figure 1. Size distribution determined by photon correlation spectroscopy of Gd_2O_3 nanoparticles after (a) synthesis and (b) the first and (c) the second growth step. (d) Size distribution of 4.6 nm sized Gd_2O_3 core embedded in a polysiloxane shell (thickness ~2 nm). The insets show the HRTEM of the corresponding particle.

Luminescence Spectra. The emission spectra were measured at room temperature with a convenient excitation wavelength. The excitation source is a 450 W xenon lamp coupled to an H10-D Jobin-Yvon monochromator with a 1200 groves/mm grating, and the emission was transferred by a fibber, placed at 45° to the sample, and recorded by an air cooled CCD camera coupled to Jobin-Yvon Trion 320 monochromator (300 g/mm, 250 nm grating, resolution = 1 nm). Light was collected with PMT (filter Kodak W2b and number 8, $\lambda < 500$ nm).

Magnetic Measurements. The magnetization curves were recorded on a magnetometer VSM-NUVO (MOLSPIN, Newcastle Upon Tyne, U.K.) at 25 °C.

NMR Spectroscopy. Proton nuclear magnetic relaxation dispersion (NMRD) profiles extending from 0.24 mT to 1.2 T were recorded with field cycling relaxometers (Field Cycling Systems, Oradell, New Jersey and Stelar, Mede, Italy) on 0.6 mL solutions contained in 10-mm o.d. tubes at 25 °C. Proton relaxation rates were also measured at 0.47, 0.94, and 1.5 T with Minispec PC-120, PC-140, and mq-60. All these instruments were from Bruker (Karlsruhe, Germany).

Relaxation Time Measurements and MR Imaging. Relaxation time measurements and MR imaging were performed at 7 T using an inversion recovery FLASH (IR-FLASH) imaging sequence with varying IR time (Biospec System 70/20, Brucker, Ettlingen, Germany). T_1-weighted contrast enhancement was performed running a standard spin−echo (SE) sequence with 500 ms TR and 12 ms TE. In vivo experiments were performed on anesthetized rats ($n = 2$; 430 g) under authorization of the regional ethic committee for animal experiment. Anaesthesia was induced with 1.8−2% isoflurane and maintained with 1.4−1.6% isoflurane in a mixture of O_2/N_2 (25/75%). MRI was conducted on a 7 T-imager (Biospec 70/20, Bruker), using a T_1-weighted sequence (TR = 40 ms, TE = 2ms, flip angle = 60°, 256 × 128 matrice, slice thickness = 2 mm). Following the acquisition of baseline MR images, nanoparticles solution was injected intravenously and dynamic MRI coronal images were obtained for each animal (maintained at normal body temperature) over 1 h. After imaging, the rats were sacrificed and dissected for determining by ICP−MS the amount of gadolinium in organs.

Fluorescence Imaging Setup. Female Swiss nude mice (6−8 weeks old, JANVIER) were anesthetized (isoflurane/oxygen 3.5% for induction and 1.5% thereafter) and were injected intravenously with 200 μL and were illuminated by 633 nm light emitting diodes (LEDs) equipped with interference filters. Fluorescence images as well as black and white pictures were acquired by a back-thinned CCD cooled camera (ORCAII-BT-512G, HAMAMATSU). A colored glass long pass filter RG 665 (MELLES GRIOT) cuts off all excitation light in the image. Fluorescence images can be superimposed on the black and white picture for better visualization of the fluorescent signal. After imaging, the mice were sacrificed and dissected for imaging organs.

Results and Discussion

Three sets of gadolinium oxide cores distinguished by their hydrodynamic diameter (3.3, 5.2, and 8.9 nm) were synthesized to study the influence of core size on MR image contrast. The smallest particles were obtained by applying a previously described protocol which consists of a direct precipitation of oxides in diethyleneglycol. The alkaline hydrolysis of $GdCl_3$ carried out in DEG at 180 °C and in substoichiometric conditions (i.e., the amount of aqueous NaOH solution added to the gadolinium salt is smaller than the stoichiometric amount) led to the formation of Gd_2O_3 nanoparticles. Their hydrodynamic diameter, determined by photon correlation spectroscopy, is 3.3 ± 0.8 nm (Figure 1a).

As expected, the hydrodynamic diameter is a bit larger than the diameter (2.2 nm) estimated from a visual examination of

Scheme 1. Schematic Illustration of the Synthesis and of the Surface Functionalization by PEG of Gadolinium Oxide Cores (with Various Sizes) Embedded in a Fluorescent Polysiloxane Shell (with X = F if Fluoresceine, R if Rhodamine, and C if Cyanine 5)

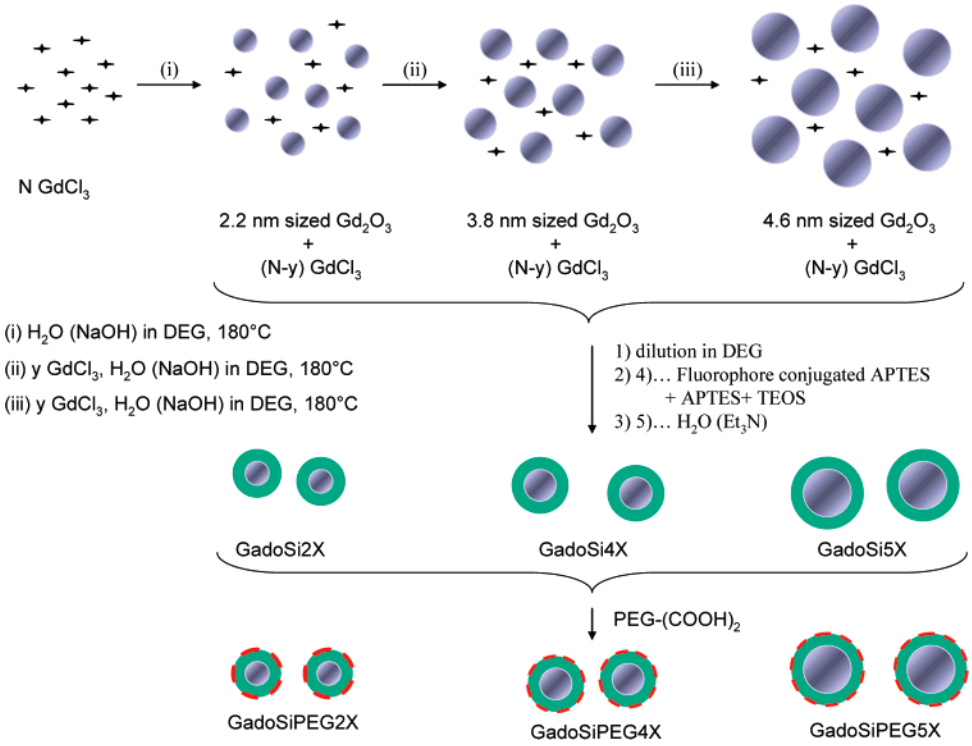

high-resolution images of transmission electron microscopy (HRTEM) since the hydrodynamic diameter is the sum of the core size and the thickness of adsorbed molecules layer. For bigger amounts of alkaline water, the appearance of turbidity reflects the presence of undesired gadolinium hydroxide aggregates. This route seems therefore not suited for the elaboration of transparent sols of gadolinium oxide nanoparticles with larger size. The increase of the core size was obtained by iterative steps starting from an aliquot of a sol containing the smallest particles which play the role of nucleation sites (Scheme 1).

The latter was poured in DEG solution containing the complement in $GdCl_3$. The alkaline hydrolysis of this mixture in substoichiometric conditions provided larger particles whose hydrodynamic diameter is 5.2 ± 1.2 nm and core size is 3.8 nm (Figure 1b). In the same way, particles with an hydrodynamic diameter of 8.9 ± 2.1 nm (core size: 4.6 nm) were obtained from an aliquot of the precedent sample (Figure 1c). Each class of Gd_2O_3 cores was embedded in a luminescent polysiloxane shell whose growth is controlled by a sequential addition of shell precursors and of an aqueous triethylamine solution to a diluted sol of Gd_2O_3 nanoparticles dispersed in DEG. The encapsulation was carried out at 40 °C for 48 h after the addition of the last portion of reagents to the sol. This fluorescent polysiloxane shell was formed by hydrolysis−condensation of a mixture of tetraethyl orthosilicate (TEOS, as reticulating agent), aminopropyltriethoxysilane (APTES), whose amino groups will serve as anchoring sites for further functionalization, and, for the first portion added, organic fluorophores (fluoresceine isothiocyanate (FITC), rhodamine B isothiocyanate (RITC), or cyanine 5 NHS ester (Cy5)) conjugated to APTES. The thickness of the shell which is fixed by the amount of reagents (shell precursors and aqueous triethylamine solution) is about 2 nm for each sample (Scheme 1 and Figure 1d). Before applying these nanoparticles for in vivo applications, a severe protocol for the purification of the nanoparticles was developed to remove the toxic Gd^{3+} ions. Their presence can also disturb the magnetic characterization of Gd_2O_3 nanoparticles (in peculiar the determination of the relaxivities) since Gd^{3+} ions possess high relaxivities related to the possibility of the latter to interact with nine water molecules, whereas gadolinium chelates are only coordinated by one or two water molecules. The undesirable presence of unreacted Gd^{3+} is due to the low conversion rate of $GdCl_3$ (around 40%) imposed by the sub-stoichiometric conditions which are required for an accurate control of the composition and the size of the Gd_2O_3 cores. To achieve this goal, four dialyzes of GadoSi2F (D1, D2, D3, D4) were successively carried out against ethanol for 7 days (D1, D2, D3 for 1 day each and D4 for 4 days) and followed up by ICP analyses.

Figure 2 depicts the evolution of the gadolinium content inside the dialysis tube during the experiment. A dramatic decrease

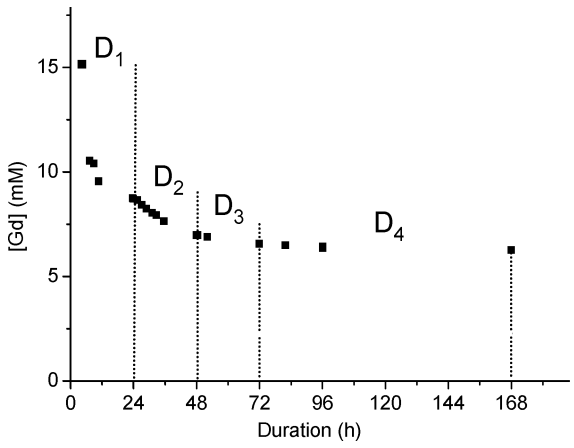

Figure 2. Evolution of the gadolinium concentration inside the dialysis tube for seven days. Vertical dotted lines correspond to the replacement of the solvent used for the dialysis.

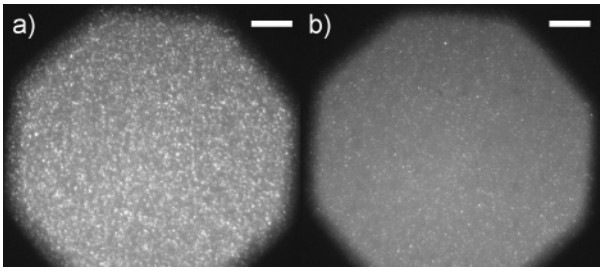

Figure 3. Optical micrographs of an aqueous colloidal solution of luminescent hybrid nanoparticles (GadoSi2F) at (a) high ([Gd] = 400 nM) and (b) low ([Gd] = 4 nM) concentrations (scale bar: 10 μm).

of gadolinium content is observed during the first 2 days (D1 and D2) before attaining a plateau at ~6 mM which is the value expected for the Gd_2O_3 synthesis with a conversion rate of 40%. The shape of the graph reflects the departure of Gd^{3+} ions through the dialysis membrane whose pore size prevents from the leakage of Gd_2O_3 nanoparticles from the dialysis tube. The plateau indicates that there is after 7 days no more free Gd^{3+} ions left in the colloidal solution. We can deduce therefore that the gadolinium element detected by ICP−MS analysis after 7 days comes only from Gd_2O_3 nanoparticles.

The encapsulation of the oxide core prior to their use was performed because the polysiloxane shell provides attractive properties which can be accurately modulated by varying the relative amount and the composition of the precursors of the inorganic network. In peculiar the use of APTES affords the opportunity to covalently anchor fluorescent organic molecules inside the polysiloxane shell (see experimental section). Their immobilization in the shell induces a shift (~20 nm) of the maximum of emission intensity toward higher wavelengths (as compared to the molecular fluorophore conjugated to APTES in a same solvent (DEG)) and an improved photostability (5.3% of intensity loss for GadoSi2F versus 32% for FITC-APTES when exposed to a laser light during 20 s). These observations reflect the environmental changes of the fluorophores which occur when they are entrapped in the polysiloxane shell.[34]

The presence of amine groups at the surface favors also the dispersion of polysiloxane coated Gd_2O_3 cores in slightly acidic aqueous solutions because the protonation of these groups provides a positive ζ-potential to the particles (+25.2 mV at pH 4.4). The electrostatic repulsion between positive particles avoids therefore the precipitation as shown in Figure 3.

The observation of a colloidal solution with a fluorescence microscope reveals the colloidal stability since luminescent centers are homogeneously and randomly dispersed even at high concentration. On the other hand the dilution of the sol shows obviously that the large light emission regions observed at high concentration (Figure 3a) results only from the superposition of luminescent restricted zones and not from the agglomeration since these zones are smaller and more dispersed after dilution (Figure 3b).

As the stability of these colloids is pH-dependent, agglomeration and precipitation, which impede their use for in vivo application, can however occur in neutral and alkaline solutions. If the aminated surface of the polysiloxane coated Gd_2O_3 nanoparticles ensures the colloidal stability in acidic solution it allows also the grafting of organic molecules. As poly(ethylene glycol) (PEG) is known for its biocompatibility, its hydrophilic, nonimmunogenic and nonantigenic character,[35] surface of hybrid

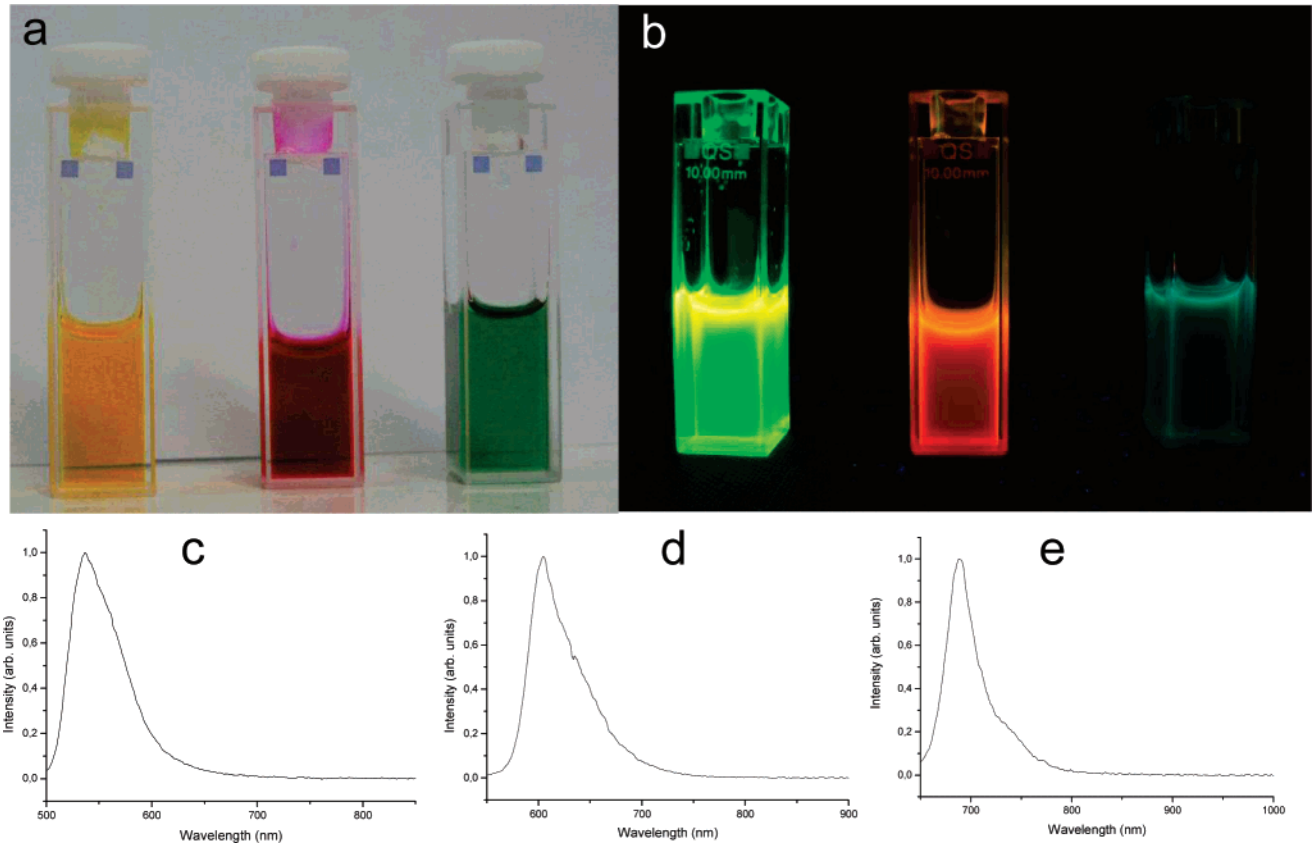

Figure 4. Photographs of aqueous solutions containing hybrid particles (from left to right) GadoSiPEG2F, GadoSiPEG2R, and GadoSiPEG2C under (a) daylight and (b) UV light; photoluminescence spectra of (c) GadoSiPEG2F (λ_{exc}= 495 nm), (d) GadoSiPEG2R (λ_{exc}= 540 nm), and (d) GadoSiPEG2C (λ_{exc}= 646 nm).

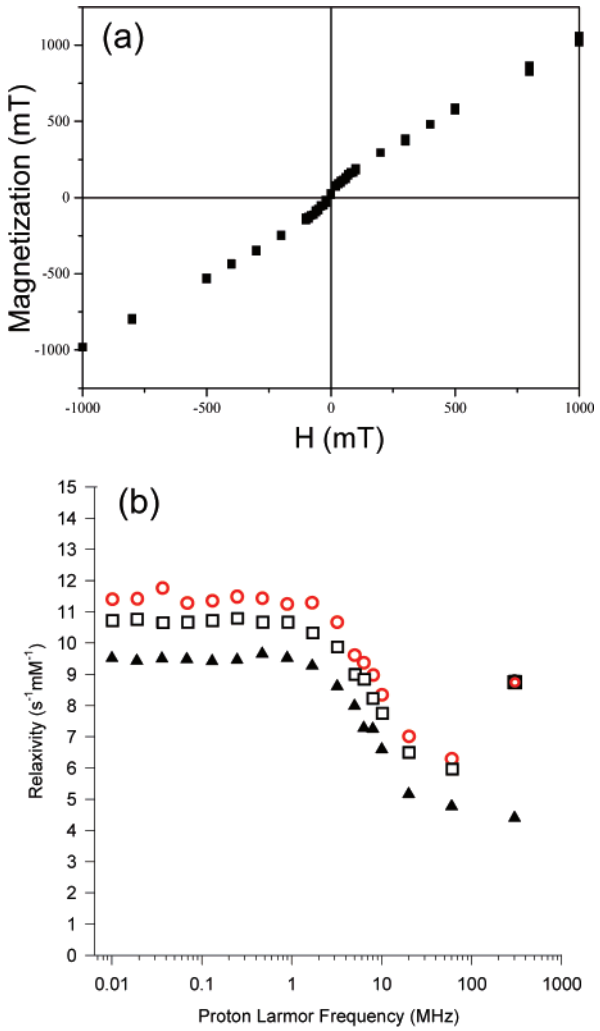

Figure 5. (a) Magnetization curve of GadoSiPEG2 at 25 °C. (b) Proton NMRD data obtained at 298 K on colloids containing GadoSiPEG2 (circles), GadoSiPEG4 (squares), and GadoSiPEG5 (triangles).

nanoparticles was derivatized by PEG. A weak molecular weight poly(ethylene glycol) with both extremities carrying carboxylic acid groups ($PEG(COOH)_2$) was grafted by one out of two ends to the aminated surface of the hybrid core−shell nanoparticles through amide linkage. Such a post-functionalization induces an increased colloidal stability in neutral and alkaline aqueous solutions owing to the carboxylate groups. The stability is ensured by electrostatic repulsion between particles since carboxylate groups confer to the particles a negative ζ-potential varying from −16 mV at pH 4 to −42 mV at pH 11. The derivatization of the surface by $PEG(COOH)_2$ makes the resulting luminescent nanoparticles suitable for in vivo applications because of their higher colloidal stability in water (Figure 4).

The field dependencies of the magnetization of GadoSiPEG2 nanoparticles are given as an example in Figure 5a, since all samples studied (Gd−DOTA and hybrid gadolinium particles) exhibit a similar behavior for $T > 50$ K. The magnetization

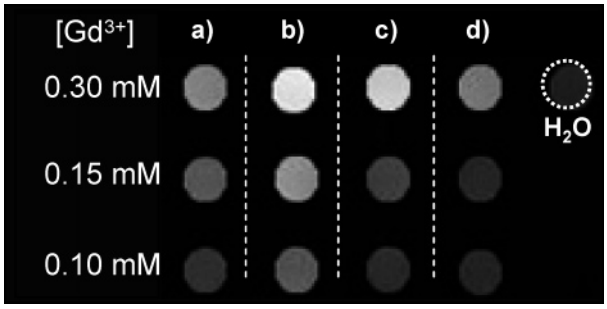

Figure 6. T_1-weighted images for various gadolinium element concentrations of (a) Gd−DOTA, hybrid nanoparticles with (b) 2.2 nm, (c) 3.8 nm, and (d) 4.6 nm sized Gd_2O_3 core ($T = 25$°C).

Table 1. Relaxivities r_1 and r_2 of Gd−DOTA and of Colloidal Solution Containing Hybrid Nanoparticles with Various Gd_2O_3 Core Sizes for a Same Gadolinium Content and for a Same Contrast Agents Number at 7 T ($T = 25$ °C)

	for a same gadolinium content		for a same contrast agents number		
sample	r_1 $(s \cdot mM)^{-1}$	r_2 $(s \cdot mM)^{-1}$	r_1 $(s \cdot mM)^{-1}$	r_2 $(s \cdot mM)^{-1}$	r_2/r_1
Gd−DOTA	4.1	4.9	4.1	4.9	1.2
Gd_2O_3, 2.2 nm	8.8	11.4	3700	4800	1.3
Gd_2O_3, 3.8 nm	8.8	28.8	18600	60700	3.4
Gd_2O_3, 4.6 nm	4.4	28.9	38800	65000	6.8

curve confirms the paramagnetic character of these water soluble nanoparticles which is commonly shared by the positive contrast agents for MRI. The proton longitudinal relaxation rates were measured at 298 K between 0.01 and 300 MHz on hybrid gadolinium oxide nanoparticles dispersed in aqueous solution (Figure 5b). In the low magnetic fields range, the longitudinal relaxivity slightly decreases when the gadolinium oxide core is larger. As the surface-to-volume ratio decreases for the largest cores, the interactions between water molecules and the gadolinium at the surface are probably less numerous inducing a longitudinal relaxivity decrease. In the case of GadoSiPEG2 and GadoSiPEG4, the longitudinal relaxivities sharply increase at high magnetic fields in good agreement with large positive contrast agents which are characterized by a slow rotation. Surprisingly this increase is not observed in this range of magnetic fields for GadoSiPEG5 (the largest cores). Although the magnetic behavior of gadolinium oxide nanoparticles is not fully elucidated since a better comprehension will require further experiments, their potential to be used as positive contrast agents for MRI which was revealed by the NMRD data is confirmed by T_1-weighted MR images recorded at 7 T. For a same gadolinium concentration (determined by ICP−MS), T_1-weighted MR images are found to be brighter when hybrid luminescent Gd_2O_3 nanoparticles are used as contrast agents instead of Gd−DOTA (gadolinium chelated by 1,4,7,10-tetraazacyclodecane-1,4,7,10-tetraacetic acid, i.e., DOTA) which is widely used in clinical MRI (Figure 6).

This is reflected by the longitudinal relaxivities r_1 values which are higher in the case of hybrid gadolinium particles (especially when the core sizes are 2.2 and 3.8 nm) than for Gd−DOTA for a same gadolinium concentration (Table 1).

It must be pointed out that the presence of the luminescent polysiloxane shell does not prevent Gd^{3+} ions in the crystalline core to exert their influence on the water protons. Two assumptions can be proposed to explain this observation. This coating is probably sufficiently porous for allowing the circula-

(34) Ow, H.; Larson, D. R.; Srivastava, M.; Baird, B. A.; Webb, W. W.; Wiesner, U. *Nano Lett.* **2005**, *5*, 113−117.
(35) (a) Harris, J. M.; Chess, R. B. *J. Am. Chem. Soc.* **2003**, *2*, 214−221. (b) Bhadra, D.; Bhadra, S.; Jain, P.; Jain, N. K. *Pharmazie* **2002**, *57*, 5−29. (c) Kohler, N.; Sun, C.; Fichtenholtz, A.; Gunn, J.; Fang, C.; Zhang, M. *Small* **2006**, *2*, 785−792. (d) Kohler, N.; Fryxell, G. E.; Zhang, N. *J. Am. Chem. Soc.* **2004**, *126*, 7206−7211.

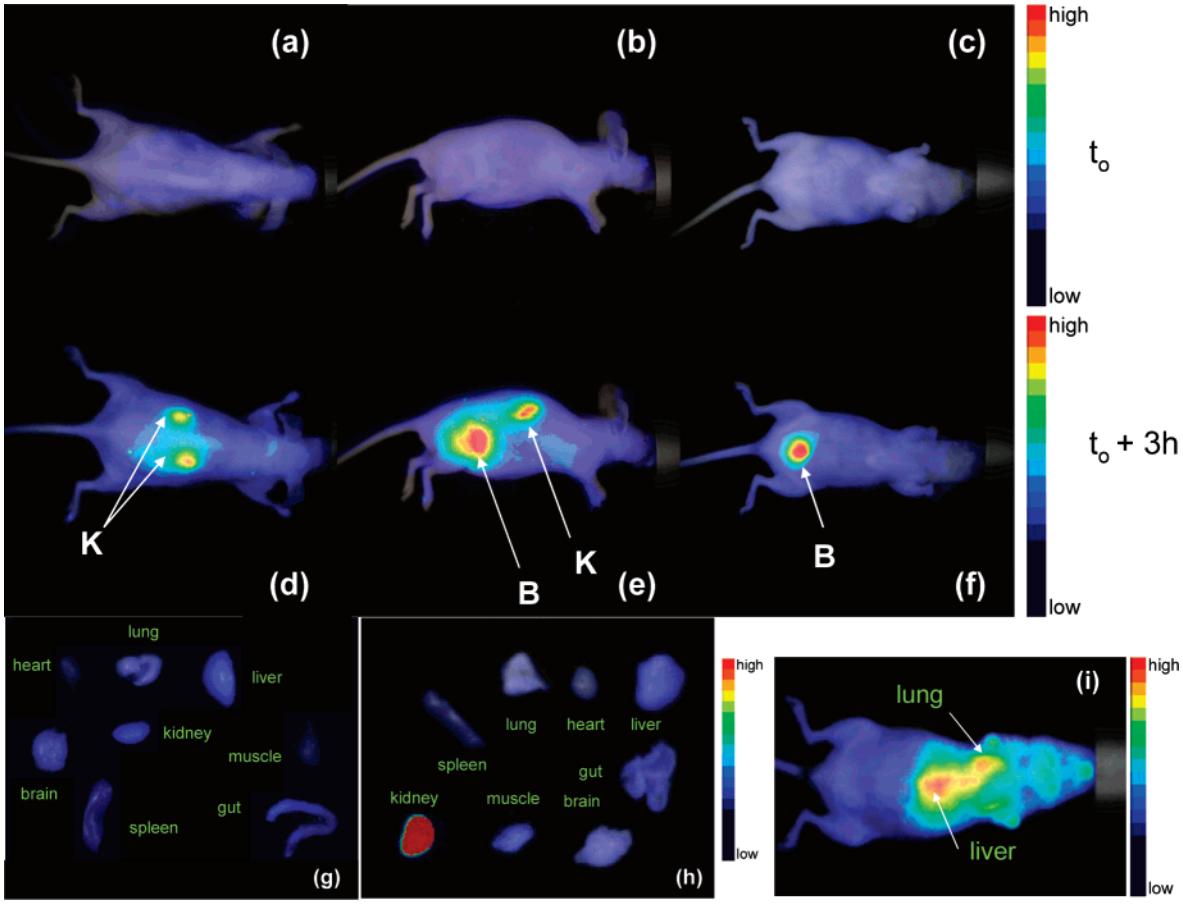

Figure 7. Fluorescence reflectance imaging of a nude mouse (a, b, c) before and (d, e, f) 3 hours after the injection of GadoSiPEG2C (K, kidneys; B, bladder). Fluorescence reflectance imaging of some organs after dissection (g) of a control mouse (no particles injection) and (h) of the nude mouse visualized on pictures (a−f). (i) Fluorescence reflectance imaging of a nude mouse after the injection of GadoSi2C (particles without PEG). Each image is acquired with an exposure time of 200 ms.

tion of water molecules from the solution to the surface of the crystalline core and/or the polysiloxane network is able to retain water molecules at the surface of the Gd_2O_3 core owing to hydrogen bonds. Moreover these values remain almost the same after at least one week. This signal stability reflects on the one hand the colloidal stability of the particles since r_1 should decrease if precipitation occurred and on the other hand the absence of gadolinium oxide core dissolution which should induce an increase of longitudinal relaxivity owing to the leakage of free Gd^{3+} ions ($r_1(Gd^{3+}) = 11.4\ mM^{-1}{\cdot}s^{-1}$). The r_1 evolution with core size seems to indicate that the effect on r_1 does not only result from the Gd^{3+} ions present at the surface of the crystalline core but also partially from those which are inside the core (Figure 5 and Table 1). Indeed the difference between relaxivities r_1 of each type of nanoparticles is expected to be more important if only the contribution of the Gd^{3+} ions at the surface was taken into account, since the number of Gd^{3+} ions at the surface of 2.2 sized Gd_2O_3 cores for a same gadolinium content is approximately 1.7 and 2 times as big as in the case of 3.8 and 4.6 nm sized Gd_2O_3 cores, respectively. It means that in the three samples all Gd^{3+} ions (except at 7 T for the largest Gd_2O_3 cores) have almost the same influence whatever their location in the crystalline structure. The studies of van Veggel and Prosser focused on GdF_3 nanoparticles already suggested that Gd^{3+} ions located beneath the outer shell of Gd^{3+} are also contributing to the relaxation.[29] In other words, even if they are not in direct contact with water, Gd^{3+} ions can exert an influence on the relaxation of water protons.

Although r_1 of the largest Gd_2O_3 core is weaker than r_1 of the smallest particles and is of the same range than r_1 of the Gd−DOTA molecules for a same gadolinium concentration, they remain very attractive for molecular imaging which supposes a specific labeling of the studied biological substrate (tissues, cells, proteins, ...). The immobilization of hybrid nanoparticles with a large Gd_2O_3 core on specific binding sites could indeed very significantly enhance the local contrast since the number of active Gd^{3+} ions (i.e., able to exert an influence on the relaxivity of water protons) is much greater as compared to small nanoparticles (in spite of a higher r_1 for a same gadolinium concentration) and to gadolinium chelates. This is reflected by normalizing the relaxivities, r_1 and r_2 to the same number of contrast agents (Table 1). Since a Gd_2O_3 core of 4.6 nm contains 8900 Gd^{3+} ions, the normalized relaxivity amounts to 38800 $s^{-1}{\cdot}mM^{-1}$, whereas it is equal to 3700 $s^{-1}{\cdot}mM^{-1}$ for a Gd_2O_3 core of 2.2 nm and remains equal to 4.1 $s^{-1}{\cdot}mM^{-1}$ for Gd−DOTA because of the presence of only one Gd^{3+} ion per chelate.

To evaluate these hybrid nanoparticles as contrast agents for FI and MRI, GadoSiPEG2C (i.e., 2.2 nm sized Gd_2O_3 core embedded in a polysiloxane shell whose inner part is functionalized by Cy5 and the outer part by PEG) was selected for intravenous injection in mice and rats. To this end, an aliquot

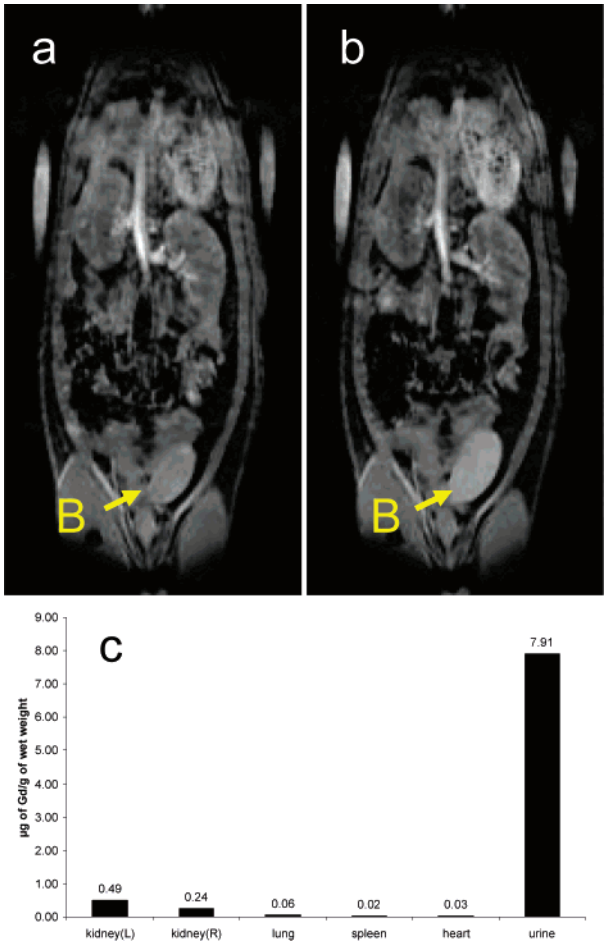

Figure 8. T_1-weighted images of rat (a) before and (b) one hour after injection of GadoSiPEG2C (B for bladder). (c) ICP−MS of some organs and urine.

of the aqueous GadoSiPEG2C colloidal solution was diluted in HEPES buffer containing 150 mM NaCl (injected volume: 100 μL for mice and 300 μL for rats). The concentration of the resulting injectable solution in gadolinium and in Cy5 amounts to 1.28 mM (0.9−2.5 μmol/kg) and 0.03 mM, respectively. Cy5 was preferred to fluorescein and to rhodamine because it possesses a higher light penetration through living tissues owing to their weak absorbance at its excitation and emission wavelengths. Despite the low content in contrast agents, the hybrid particles could be detected (Figures 7 and 8).

The injection of GadoSiPEG2C in mice was monitored for 3 h by FI thanks to an optical setup that allows imaging of the whole mouse. The set of images taken at various times (between 0 (just before injection) and 180 min) after injection and for various position (mice were laid on abdomen, on the left side and on back) shows obviously that particles accumulated in the kidneys and in the bladder (Figure 7a−f). It must be emphasized that no undesirable uptake in lung and liver was detected. This biodistribution was confirmed by the visualization under excitation light of the organs after dissection since no light is emitted from the organs except kidneys which emit intense light (Figure 7g−h). The follow-up by MRI of the circulation of these particles injected in rats yielded identical results (Figure 8).

One hour after the injection, nanoparticles accumulated in the bladder, which became brighter as shown Figure 8b. The post-mortem ICP analysis of the organs confirmed that gadolinium element was essentially present in urine and kidneys (Figure 8c). The uptake in lung, spleen and heart was quite insignificant (Figure 8c). This observation indicates that hybrid luminescent particles are able to circulate in the vessels for at least 3 h without aggregation since no uptake was observed in the lung, which is drained by quite very thin capillaries. Moreover the absence of luminescent particles in the liver shows low-recognition by the immune system and that the particles were naturally eliminated by renal excretion. This safe behavior is attributable to the small size of the particles but also to the pegylated corona since the injection of similar particles devoid of PEG led to the accumulation in the liver and in the lung (Figure 7i). The free circulation without undesirable accumulation in living bodies of these probes (GadoSiPEG2C), combining fluorescence imaging and MRI, allows us to envisage their use for specific accumulation in targeted tissues since the surface of these hybrid particles have proven to be functionalized by biotargeting groups.[31,35]

Conclusion

This study shows that gadolinium oxide core embedded in a polysiloxane shell whose inner part is functionalized by organic dyes and the outer part by PEG are well suited for in vivo dual modality magnetic resonance and fluorescence imaging. The gadolinium oxide core induces an enhancement of the positive contrast of MR images as compared to widely used contrast agents in clinical MRI, whereas the fluorescence imaging results from the presence of organic dyes in the polysiloxane shell. The data reveal that the longitudinal relaxivity per particle increases with the core size. We have demonstrated in a previous paper that these hybrid nanoparticles can be derivatized by biotargeting groups.[31] Because of their bioavaibility and very high relaxivity per particle demonstrated in this study, they could then be useful for molecular imaging purpose, which requires a strong local contrast enhancement. As ^{157}Gd (natural abundance ∼20%) possesses a high neutron capture cross-section (66 times higher than ^{10}B), these particles also appear as a good alternative to boron compounds for neutron-capture therapy. This alternative therapy would consist of destroying the hybrid Gd_2O_3 nanoparticles loaded tumor with energetic particles resulting from an interaction between the internalized biocompatible nanoparticles and a harmless thermal neutron beam. Experiments aiming at the development of hybrid Gd_2O_3 nanoparticles combining dual modality imaging for diagnostic and neutron-capture therapy are in progress.

Acknowledgment. This work was supported by a grant from the regional council of Rhône-Alpes (France) and by ANR-05-NANO-037-02. S.L., L.V.E., and R.N.M. thank the FNRS and the ARC Program 00/05-258 of the French Community of Belgium for financial support. The support and sponsorship concerted by COST Action D18 "Lanthanide Chemistry for Diagnosis and Therapy" are kindly acknowledged. The fluorescence microscopy on colloidal sample was performed by Dr. Christophe Place (Laboratoire Joliot-Curie, Département de Physique, UMR CNRS 5672 Ecole Normale Supérieure de Lyon).

JA068356J